



# Structure, piezoelectric, ferroelectric and dielectric properties of lead-free ceramics $0.67\text{BiFeO}_3-0.33\text{BaTiO}_3-x\text{BiGaO}_3+0.0035\text{MnO}_2$

Shibo Guan<sup>1,2</sup> · Huabin Yang<sup>1,2</sup> · Rui Zhang<sup>1,2</sup> · Jinyuan Pang<sup>1,2</sup> · Minhong Jiang<sup>1,2</sup> · Yuanyuan Sun<sup>1,2</sup>

Received: 5 April 2018 / Accepted: 30 July 2018 / Published online: 11 August 2018  
© Springer Science+Business Media, LLC, part of Springer Nature 2018

## Abstract

BF–BT–*x*BGa (shortened for  $0.67\text{BiFeO}_3-0.33\text{BaTiO}_3-x\text{BiGaO}_3+0.0035\text{MnO}_2$ ) lead-free piezoelectric were prepared by a conventional solid-state sintering method. The phase structure, miscostructure, piezoelectric, ferroelectric and dielectric properties were investigated. BiGaO<sub>3</sub> doping has little effect on the crystal structure of BF–BT–*x*BGa lead-free piezoelectric ceramics. All samples are perovskite structure. With the change of *x*, the structure of the sample is pseudo cubic structure. The ceramics (with *x*=0.02 sintered at 990 °C) has  $P_r=25\ \mu\text{C}/\text{cm}^2$ ,  $E_c=22.059\ \text{kV}/\text{cm}$  and high depolarization temperature  $T_d=422\ ^\circ\text{C}$ . It was found that the piezoelectric properties of the ceramic were improved by addition of BiGaO<sub>3</sub>. The ceramic shows excellent electrical properties when *x* is 0.02:  $d_{33}=170\ \text{pC}/\text{N}$  and  $T_c=434\ ^\circ\text{C}$ . Proper amount of BiGaO<sub>3</sub> doping can improve the size of the crystal and promote the sintering of samples. These results show that the addition of BiFeO<sub>3</sub>–BaTiO<sub>3</sub> based ceramics is promising lead-free piezoelectric ceramics for practical applications.

## 1 Introduction

Piezoelectric ceramic is a kind of polycrystalline material with mechanical and electrical energy conversion function. It has a wide range of applications in medicine, industry, aerospace and other fields [1–4]. Lead zirconate titanate (PZT) based ceramics have attracted much attention due to their good piezoelectric and electromechanical coupling properties [5–8]. However, lead toxicity poses a serious threat to human health and the environment, so it has led us to constantly search for other lead free alternatives [9]. Hexagonal  $\text{PbCr}_x\text{Fe}_{12-x}\text{O}_{19}$  nanostructures were prepared by sol–gel self combustion method [10]. La<sup>3+</sup> doped  $\text{ZnFe}_2\text{O}_4$  nanostructures were prepared by a 2-step sol–gel process [11]. Ziarati et al. have proved the preparation of ultrasound. The rare earth element based on ferrite and  $\text{NiFe}_{2-x}\text{Eu}_x\text{O}_4$  is an effective catalyst for the synthesis of benzimidazole, benzoxazole and benzothiazole under ultrasonic irradiation

[12]. Rahimi-Nasrabadi et al. have been reported that  $\text{CuFe}_{2-x}\text{Ce}_x\text{O}_4$  nanoparticles were successfully synthesized by simple self combustion sol–gel method [13].

BiFeO<sub>3</sub> has recently gained considerable interest both technologically and scientifically due to the existence of both ferroelectric and (anti)ferromagnetic ordering in the same phase in the material [14–17]. Bi<sub>2</sub>Fe<sub>4</sub>O<sub>9</sub>, Bi<sub>46</sub>Fe<sub>2</sub>O<sub>72</sub> and other heterozygous phases will be produced in the preparation of BiFeO<sub>3</sub> by the traditional solid state sintering method [18–21]. The ionic radius of Ba<sup>2+</sup> in BaTiO<sub>3</sub> is 1.61 Å (CN=12) and the ionic radius of Ti<sup>4+</sup> is 0.605 Å (CN=6) [22]. BaTiO<sub>3</sub> has a low tetragonal–cubic transition temperature. This tetragonal perovskite phase is stable over an extended temperature range, so it has good piezoelectric properties as a ferroelectric material ( $d_{33}\sim 400\ \text{pC}/\text{N}$ ) [23]. However, its lower Curie temperature  $T_c\sim 130\ ^\circ\text{C}$  hindered its application. In general, BaTiO<sub>3</sub>-based lead-free piezoelectric ceramics have the advantages of high piezoelectric constant, high dielectric constant, large electromechanical coupling coefficient, mechanical quality factor and small dielectric loss. However, it has the disadvantages of low Curie temperature, high sintering temperature and strong sensitivity of the piezoelectric properties to temperature changes.

In addition, many researchers have studied the crystal structure of the  $(1-x)\text{BiFeO}_3-x\text{BaTiO}_3$  ceramic system, but the results of the study are different. By changing the

✉ Huabin Yang  
495221054@qq.com

<sup>1</sup> School of Material Science and Engineering, Guilin University of Electronic Technology, Guilin 541004, Guangxi, People's Republic of China

<sup>2</sup> Guangxi Key Laboratory of Information Materials, Guilin University of Electronic Technology, Guilin 541004, Guangxi, People's Republic of China

stoichiometry of  $\text{BiFeO}_3$  and  $\text{BaTiO}_3$  in  $(1-x)\text{BiFeO}_3-x\text{BaTiO}_3$  ceramic system, Kumar et al. found that the crystal structure and lattice parameters of  $(1-x)\text{BiFeO}_3-x\text{BaTiO}_3$  ceramic system were closely related to the stoichiometry of  $\text{BiFeO}_3$  and  $\text{BaTiO}_3$  [24]. In 2009, Leontsev and Eitel reported that Mn doped  $(1-x)\text{BiFeO}_3-x\text{BaTiO}_3$ , at  $x=0.25$ , the piezoelectric coefficient  $d_{33}$  reached 116 pC/N, and its ferroelectric transition temperature was above 450 °C [25]. In 2015, Lee et al. studied  $(1-x)[0.67\text{Bi}_{1.05}\text{FeO}_3-0.33\text{BaTiO}_3]-x\text{Bi}_{1.05}(\text{Zn}_{0.5}\text{Ti}_{0.5})\text{O}_3$  ( $x=0.03$ , BF33BT–3BZT) and  $0.67\text{Bi}_{1.05}(\text{Fe}_{1-x}\text{Ga}_x)\text{O}_3-0.33\text{BaTiO}_3$  ( $x=0.03$ , BF33BT–3BG) piezoelectric ceramics. The piezoelectric constant  $d_{33}$  and the Curie temperature  $T_c$  are respectively BZT (BF33BT–3BZT,  $d_{33}=324$  pC/N,  $T_c=466$  °C) and BG (BF33BT–3BG,  $d_{33}=402$  pC/N,  $T_c=454$  °C) [26].  $\text{BiFeO}_3$ – $\text{BaTiO}_3$  has been shown to have excellent piezoelectric properties and high temperature resistance. Zhou et al. has been studied that Ga doped  $\text{BiFeO}_3$ – $\text{BaTiO}_3$  lead-free piezoelectric ceramics. It was found that a small amount of Ga could improve the grain size and piezoelectric properties of the sample ceramics [27]. In this work, the ceramics of  $\text{BiGaO}_3$  doped BF–BT– $x\text{BGa}$  solid solution were prepared by conventional sintering technique. The microstructure, the piezoelectric properties, ferroelectric properties, dielectric properties and thermal stability of the ceramics were investigated.

## 2 Experimental procedures

BF–BT– $x\text{BGa}$  ceramics were prepared by a conventional ceramic fabrication technique. Reagent-grade oxide of  $\text{Bi}_2\text{O}_3$  (99.99%),  $\text{Fe}_2\text{O}_3$  (99.2%),  $\text{TiO}_2$  (99.99%),  $\text{BaCO}_3$  (99.99%), and  $\text{MnO}_2$  (99.99%) were used as the starting materials. The mixture was ball milled with addition of alcohol for 24 h. The samples were dried at a temperature of 800 °C for 4 h after drying, drying and screening after adding PVA binder. The samples were heated to 600 °C by sintering 4 h for the glue, then sintered for 2 h at 970–1010 °C. The crystal structure of the sample was detected by XRD (D8 Advance; Bruker Inc., Karlsruhe, Germany). The surface morphology of the sample was observed by scanning electron microscope (SEM, JSM-5610LV, JEOL, Japan). The piezoelectric properties and dielectric properties were measured by the quasi static  $d_{33}$  tester (ZJ-3A, CAS, Shanghai, China) and the precision impedance analyzer (4294A, Agilent). The polarization–electric field ( $P$ – $E$ ) loops at room temperature was characterized by a ferroelectric tester (Premier II, Radiant Technologies Inc., Albuquerque, NM, USA). The temperature spectrum was measured by the intelligent temperature control system and the precision impedance analyzer (4294A, Agilent). The depolarization temperature of the sample was measured by *ex situ* depolarization method.

## 3 Results and discussion

Figure 1a shows the X-ray diffraction patterns of BF–BT– $x\text{BGa}$  ( $x=0, 0.01, 0.02, 0.03, 0.04$ ) system piezoelectric ceramics at 10°–80°. All the samples were characterized by XRD. The characteristic peaks were (100), (110), (111), (200), (210), (211), (220), (221), (310), and some small clutter peaks were observed in the XRD pattern, indicating that impure phase was formed. These small clutter peaks represent  $\text{Bi}_2\text{Fe}_4\text{O}_9$ . All sample ceramics are perovskite structure. According to the 20-0169 JCPDS card number [28], we know that pure  $\text{BiFeO}_3$  is a three party structure. According to the 5-626 JCPDS card number [29], we know that pure  $\text{BaTiO}_3$  is a tetragonal structure. In this paper, the pseudo cubic structure of samples shows that the mixture of  $\text{BiFeO}_3$  and  $\text{BaTiO}_3$  can form pseudo cubic structure. Figure 1b was shown the BF–BT– $x\text{BGa}$  ( $x=0, 0.01, 0.02, 0.03, 0.04$ ) piezoelectric ceramic at 36°–50° XRD diffraction pattern. It can be seen from the figure that the (111) single diffraction peak at about 39° and the (200) single diffraction peak at 46° indicate that the crystal structure of the ceramic sample does not change significantly with

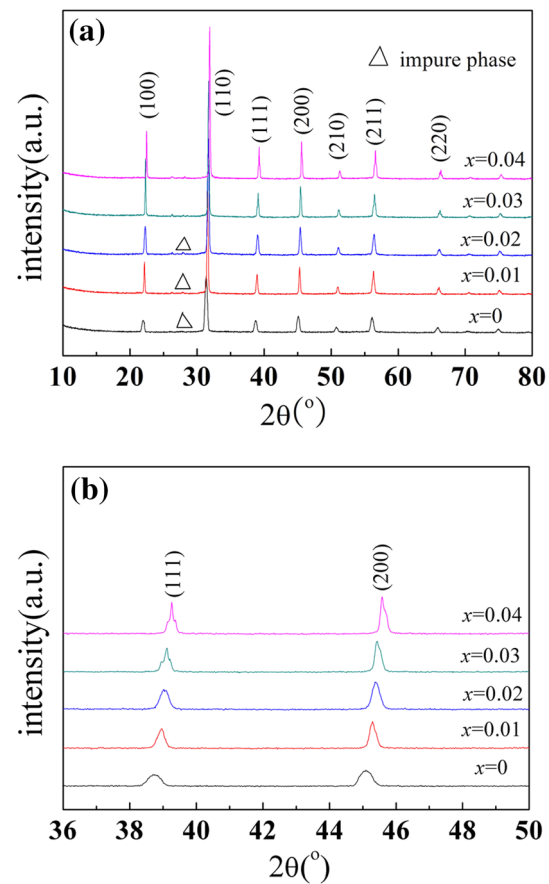


Fig. 1 XRD pattern of the BF–BT– $x\text{BGa}$  ceramics

the increase of  $x$ . It is a pseudo-cubic structure. With the increase of  $x$ , the height of the peaks at  $39^\circ$  and  $46^\circ$  increases gradually and moves to a high angle. It indicates that the spacing of crystal structure decreases gradually. The lattice parameters of BF–BT– $x$ BGa are shown in Table 1. With the increase of  $x$ , the lattice parameters ( $a$ ,  $b$ ,  $c$ ) gradually decrease, and the intersection angle ( $\alpha=90$ ,  $\beta=90$ ,  $\gamma=120$ ) remain unchanged. It is obvious that the doping of BGa has little effect on the lattice parameters of the sample ceramics.

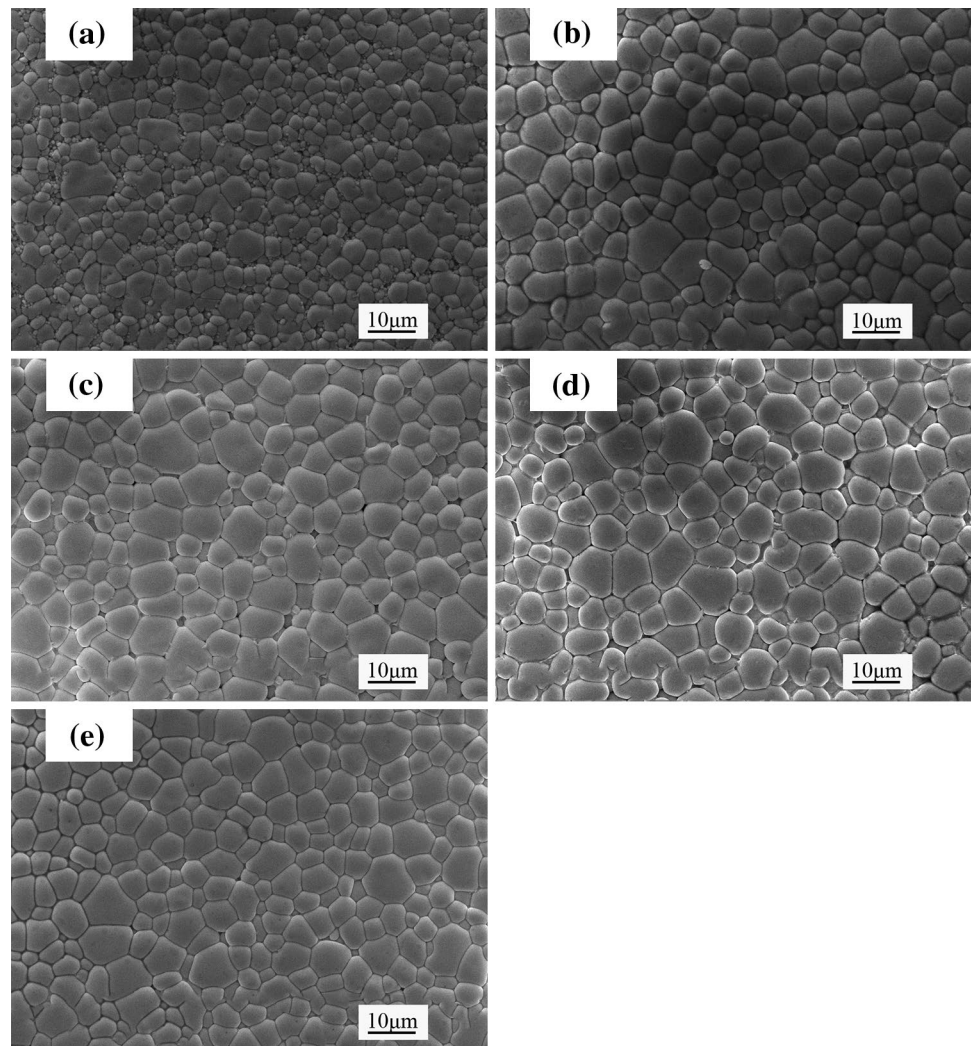
Figure 2 is the micromorphology of BF–BT– $x$ BGa piezoelectric ceramics at different Ga doping ( $x=0, 0.01, 0.02, 0.03, 0.04$ ).

It can be seen from the diagram that all the surfaces of the samples become denser, and no obvious holes are formed. The grains are regular polygons, some of them are diamond shaped, and the grain boundaries are clearer. When  $x$  is 0, the average grain size is about  $3.6 \mu\text{m}$ , indicating that the doping of Ga increases the grain size of the ceramic. when the doping amount  $x$  is 0.01 or 0.02, the grains grow gradually, the average grain size ( $x=0.02$ ) reach about  $7.2 \mu\text{m}$ . It is probable that with the increase of Ga content, the intergranular mobility increases during the sintering process, which promotes the movement of the

**Table 1** The lattice parameter for BF–BT– $x$ BGa

$x$	$a$ (Å)	$b$ (Å)	$c$ (Å)	$a$ (°)	$\beta$ (°)	$\gamma$ (°)
0	5.6623(9)	5.6623(9)	6.9707(8)	90	90	120
0.01	5.6515(7)	5.6515(7)	6.9343(7)	90	90	120
0.02	5.6455(9)	5.6455(9)	6.9446(9)	90	90	120
0.03	5.6385(5)	5.6385(5)	6.9370(1)	90	90	120
0.04	5.6342(7)	5.6342(7)	6.8709(6)	90	90	120

**Fig. 2** SEM images of BF–BT– $x$ BGa ceramics



grain boundaries and increases the grain size. This indicates that Ga doping in a certain range is conducive to the growth of ceramic sample grains. When  $x$  exceeds 0.02, the grain size of the sample ceramics decreases. This may be because excessive Ga accumulates around the grain boundaries, hindering the grain growth.

Figure 3 is a EDS diagram of BF–BT– $x$ BGa ( $x=0.02$ ) piezoelectric ceramics. From the graph, we can see that when  $x=0.02$ , the weight percentage of Ga is 0.84%, and the atomic percentage is 0.70%. We can conclude that the percentages of Ga elements in the samples are relatively low.

Figure 4a shows the  $d_{33}$  variation of Ga-doped BF–BT– $x$ BGa under different compositions of different temperatures. From the figure we can see that the  $d_{33}$  value of the sample first increases and then decreases with the increase of temperature and reaches the maximum at 990 °C. When the composition point is  $x=0.02$  and the sintering temperature is 990 °C, the  $d_{33}$  reaches 170 pC/N. This is mainly due to the increase of sintering temperature, which is beneficial to increase the density of ceramics and grain size. The increase of grain size is conducive to the turning of domain in polarization, which makes the anisotropy produced after polarization decrease, and the polarization effect increase, resulting in the increase of extrinsic piezoelectric properties. However, the increasing temperature easily leads to the volatilization of Bi, resulting in oxygen vacancies. At the same time, the density is reduced, the intrinsic piezoelectric properties are reduced and the total piezoelectric properties are decreased. Figure 4b, c shows the relationship between the piezoelectric constant  $d_{33}$ , the electromechanical coupling coefficient  $k_p$  and the mechanical quality factor  $Q_m$  of the BF–BT– $x$ BGa piezoelectric ceramic at 990 °C with the content of the doping element Ga. From the diagram, we can see that  $d_{33}$ ,  $k_p$  and  $Q_m$  increase first and then decrease with the increase of  $x$ , and reach the maximum  $d_{33}=170$  pC/N,  $k_p=0.306$  and  $Q_m=42.877$  at  $x=0.02$ .

Figure 5 shows the dielectric constant and dielectric loss of Ga-doped BF–BT– $x$ BGa piezoelectric ceramics at room temperature in relation to  $x$ . As is shown in Fig. 5a, the dielectric constant decreases firstly with the amount of BGa doping, reaches the minimum ( $\epsilon_r=620.79$  at  $x=0.02$ ), and then increases further with the increase of  $x$ . Dielectric loss also decreases with the increase of  $x$ , reaches the minimum ( $\tan\delta=0.053$  at  $x=0.02$ ), and then increases gradually with the increase of  $x$ .

Figure 6 shows the hysteresis loop of BF–BT– $x$ BGa lead-free piezoelectric ceramics under AC electric field of 30–60 kV/cm. From the figure we can see that when the polarization electric field is 30 kV/cm, the hysteresis loop is not saturated and becomes a flat ellipse. With the increase of the polarization voltage, the hysteresis loop becomes saturated gradually, and the shape evolves into a rectangle gradually, the remanent polarization of the sample increases gradually, indicating that as the polarization electric field gradually increases to 60 kV/cm, the ferroelectric properties of the sample increase gradually. On the other hand, under the same electric field, with the increase of  $x$ , the ferroelectric properties of the samples increase firstly and then decrease gradually. Figure 6f is the change of  $P_r$  and  $E_c$  of BF–BT– $x$ BGa lead-free piezoelectric ceramics with the increase of  $x$  at 60 kV/cm. As is shown in the figure, the coercive field  $E_c$  first decreases with the increase of  $x$ , reaches the minimum ( $E_c=22.059$  kV/cm at  $x=0.02$ ). As  $x$  increases,  $E_c$  increases to  $E_c=24.03$  kV/cm at  $x=0.04$ . The remanent polarization  $P_r$  increases with the increase of  $x$  and reaches the maximum of ( $P_r=25$   $\mu\text{C}/\text{cm}^2$  at  $x=0.02$ ), then decreases with the increase of  $x$ . It is indicated that the proper doping of Ga can improve the remanent polarization of BF–BT– $x$ BGa sample ceramics and improve the ferroelectric properties.

Figure 7a–e shows the relative permittivity  $\epsilon_r$  and dielectric loss  $\tan\delta$  of BF–BT– $x$ BGa system lead-free piezoelectric ceramics at 1, 10 and 100 kHz with temperature.

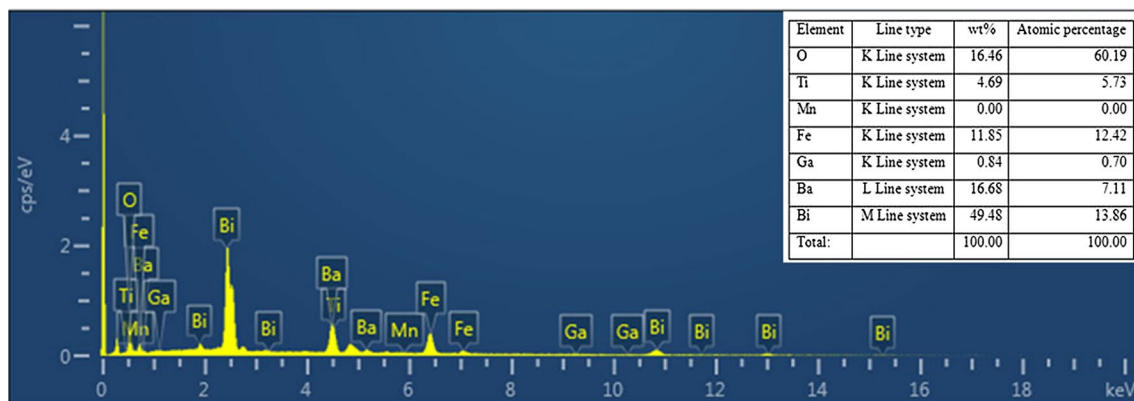
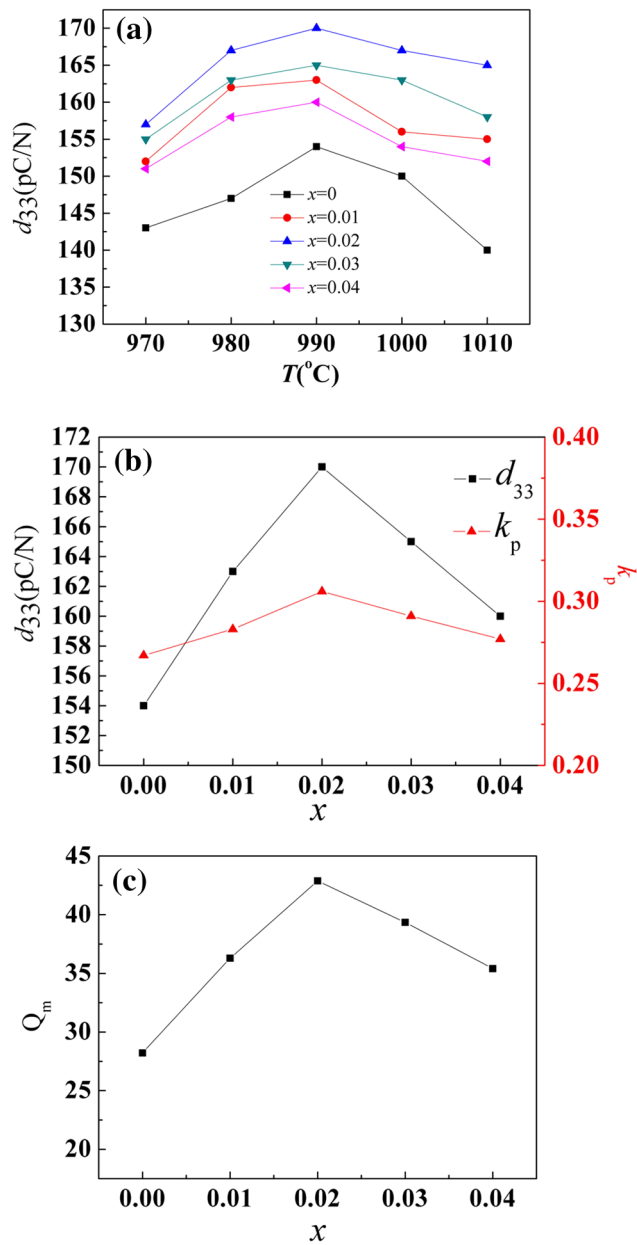
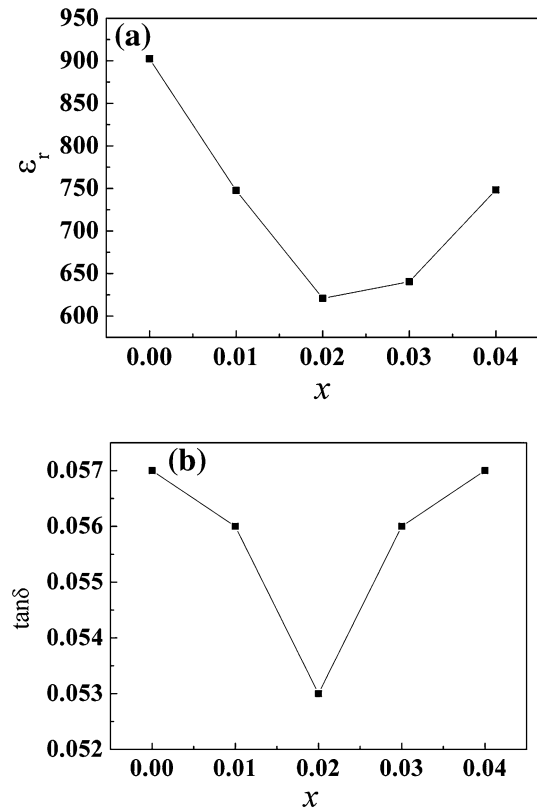


Fig. 3 EDS analysis of BF–BT– $x$ BGa ceramics



**Fig. 4** Piezoelectric constant  $d_{33}$ , the planar electromechanical coupling factor  $k_p$  and mechanical quality factor  $Q_m$  for the BF-BT- $x$ BGa ceramics

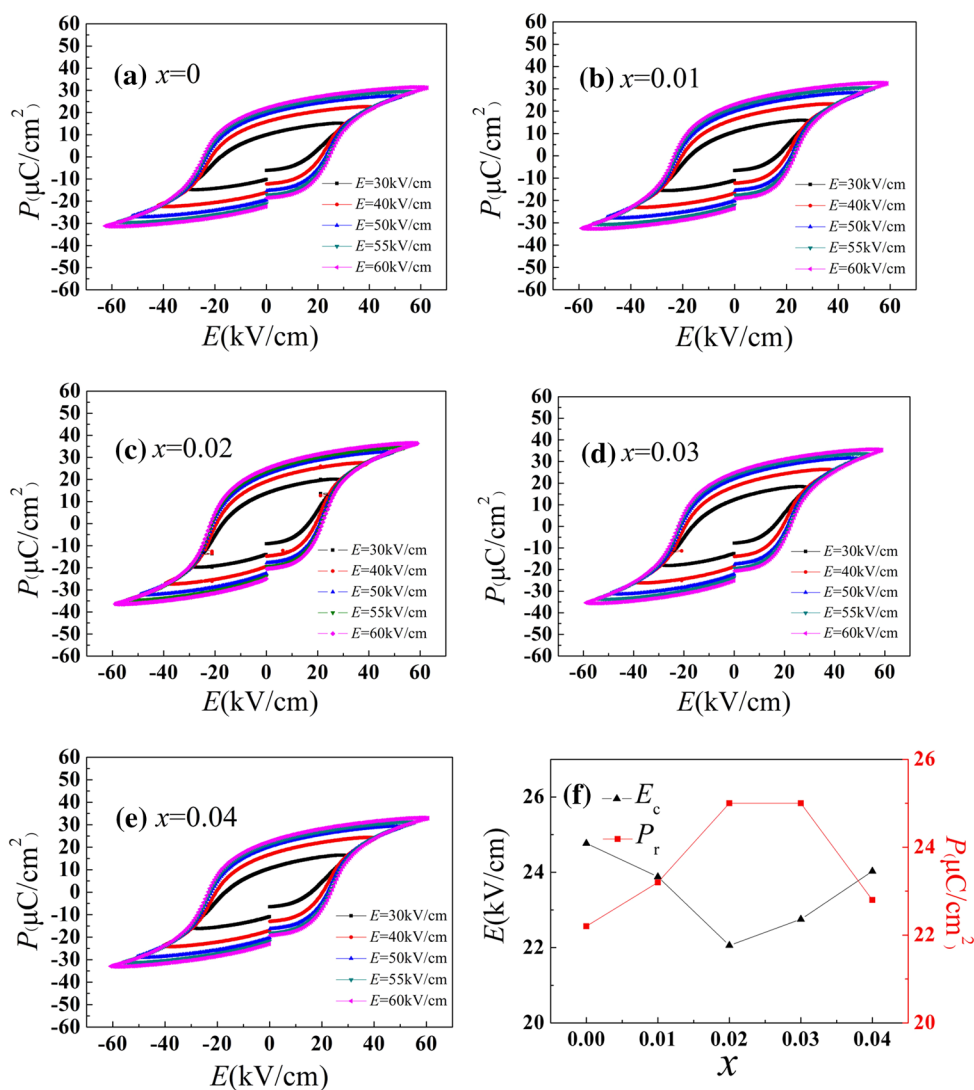
From the relationship between dielectric constant  $\epsilon_r$  and temperature, we can see that all the samples have a high-temperature dielectric anisotropy peak at high temperature, and ferroelectric phase transit to paraelectric phase at the dielectric anomalous peak. The frequency dependence at low temperature is not very obvious. With the increase of temperature, the frequency dependence becomes more and more obvious. With the increase of temperature, the frequency dependence decreases. At the high temperature dielectric anomalous peak temperature  $T_m$ , the dielectric



**Fig. 5** The relative dielectric constant  $\epsilon_r$  and dielectric loss  $\tan\delta$  of the BF-BT- $x$ BGa ceramics at room temperature

constant decreases with increasing frequency and moves to the high temperature as the frequency increases. Ferroelectrics can be divided into normal ferroelectrics, diffused ferroelectrics and relaxation ferroelectrics. Normal ferroelectrics show a sharp phase transition peak; diffuse ferroelectrics show a broad peak. The relaxor ferroelectrics show a wide peak and the Curie point moves towards the high temperature as the frequency increases. It can be seen from the figure that as  $x$  increases, the sample changes from normal ferroelectric to relaxed ferroelectrics gradually. On the other hand, it can be seen from the relationship between the dielectric loss and the temperature that the dielectric loss of the sample is low at low temperature and the frequency dependence is not obvious. With the increase of temperature, when it reaches a certain temperature, the dielectric loss increases sharply. The dielectric loss at low frequency is larger than that at high frequency, and the frequency dependence is obvious. Figure 7f shows the BF-BT- $x$ BGa system of lead-free piezoelectric ceramic Curie temperature with composition  $x$  changes. We can see from the figure, the Curie temperature increases with the increase of  $x$  and then decreases from 434 to 404 °C. The Curie temperature  $T_c$  decline may be due to the doping of Ga in the grain boundary precipitation, resulting in the

**Fig. 6** The  $P$ – $E$  hysteresis loop of the BF–BT– $x$ BGa lead-free piezoelectric ceramics with different BGa content at the 30–60 kV/cm electric field, **a**  $x=0$ , **b**  $x=0.01$ , **c**  $x=0.02$ , **d**  $x=0.03$ , **e**  $x=0.04$ , **f** the coercive field  $E_c$  and residual polarization  $P_r$  of BF–BT– $x$ BGa lead-free piezoelectric ceramics as a function of BGa doping  $x$

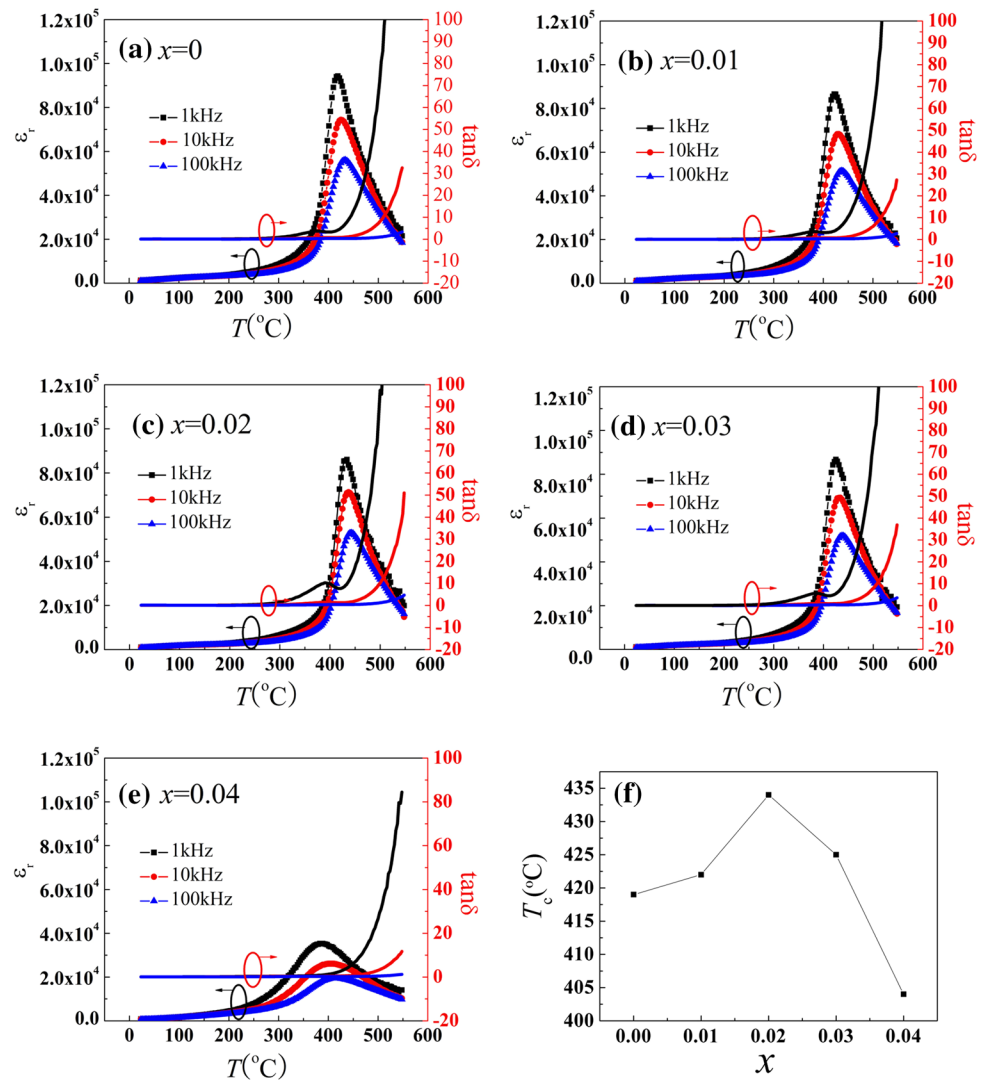


dielectric properties of ceramics decreases and reducing the Curie temperature ( $T_c$ ).

Figure 8a shows the depolarization curves of BF–BT– $x$ BGa ( $x=0, 0.01, 0.02, 0.03, 0.04$ ) system lead-free piezoelectric ceramics. We used the method of *ex situ* measurement  $d_{33}$  to measure the depolarization temperature. As is shown in the figure, the piezoelectric constant  $d_{33}$  of samples with different compositions changes little with the increase of temperature at low temperature. When the temperature increases further,  $d_{33}$  decreases gradually with the increase of temperature. When it reaches a certain temperature, the  $d_{33}$  decreases rapidly. This temperature is the critical temperature (depolarization temperature). Figure 8b is a diagram of the variation of the depolarization temperature of the lead-free piezoelectric ceramics in the BF–BT– $x$ BGa system with the change of  $x$ . From the diagram we can see that with the increase of  $x$ , the

depolarization increases first and reaches the maximum of ( $T_d=422$  °C at  $x=0.02$ ). The  $d_{33}$  of the same component point decreases with the increase of temperature. Piezoelectric ceramics only have polarized electric field to polarize, so that the electrical domain is aligned in the direction of polarization electric field, or most of the domains are aligned in the direction of polarized electric field. With the increase of temperature, the electric domain rearranged by the polarized electric field has a tendency to revert to the original disorderly arrangement, which makes the ceramic depolarize. The lower the stability of the domain after polarization, the lower the depolarization temperature. On the other hand, the higher the stability of the domain after polarization, the higher the depolarization temperature. It is found that the doping of Ga is beneficial to the improvement of the domain stability of the samples after polarization.

**Fig. 7** The temperature dependence of  $\epsilon_r$  and  $\tan\delta$  for BF–BT– $x$ BGa ceramics with  $\text{BiGaO}_3$  content at 1, 10, 100 kHz, **a**  $x=0$ , **b**  $x=0.01$ , **c**  $x=0.02$ , **d**  $x=0.03$ , **e**  $x=0.04$ , **f** Curie temperature ( $T_c$ ) as a function of  $x$  for the BF–BT– $x$ BGa ceramics



## 4 Conclusions

In this paper, the effects of Ga doping on the phase structure, morphology, piezoelectric ferroelectric properties and temperature stability of BF–BT– $x$ BGa system lead-free piezoelectric ceramics have been studied systematically. Proper amount of Ga doping can increase the piezoelectric constant  $d_{33}$ , electromechanical coupling coefficient  $k_p$  and mechanical quality factor  $Q_m$ , reduce dielectric loss, and get  $d_{33} = 170$  pC/N,  $k_p = 0.306$ ,  $Q_m = 42.877$ ,  $\tan\delta = 0.053$  at  $x = 0.02$ . When  $x = 0.02$  at  $E = 60$  kV/cm, the ceramics

obtained the coercive field ( $E_c = 22.059$  kV/cm), and the remanent polarization get  $P_r = 25$   $\mu\text{C}/\text{cm}^2$ . The temperature makes the lead-free piezoelectric ceramics of BF–BT– $x$ BGa system change from normal ferroelectric to diffused ferroelectrics, and the temperature of depolarization increases firstly and then decreases, which indicates that proper Ga can improve the temperature stability of samples. These excellent properties show that BF–BT– $x$ BGa lead free piezoelectric ceramic is a potential lead free piezoelectric material.

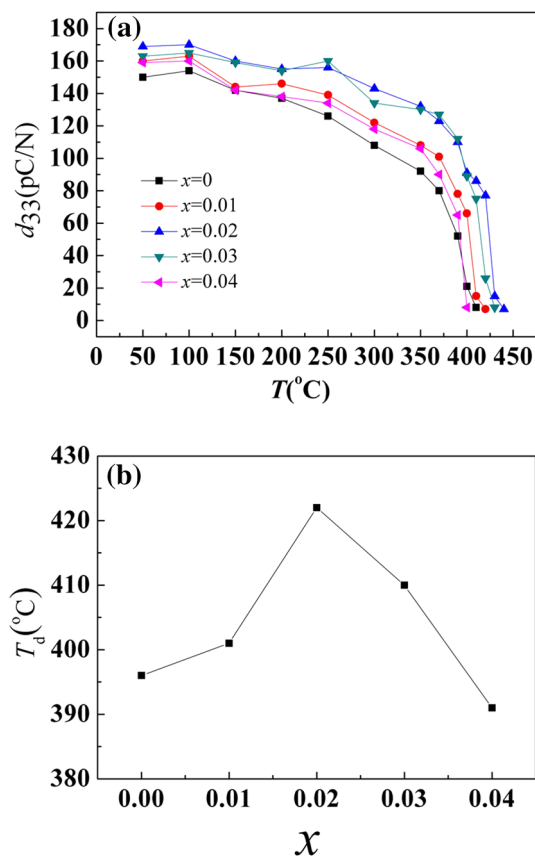


**Fig. 8** **a** The piezoelectric constant  $d_{33}$  of BF–BT– $x$ BGa lead-free piezoelectric ceramics as a function of temperature for doping different BGa contents. **b** The depolarization temperature  $T_d$  as a function of  $x$  for the BF–BT– $x$ BGa ceramics

**Acknowledgements** This work was financed by the National Natural Science Foundation of China (11364008) and the Natural Science Foundation of Guangxi (2014GXNSFAA118311) and Guangxi Key Laboratory of Information Materials.

## References

- V.F. Janas, A. Safari, *J. Am. Ceram. Soc.* **78**, 2945 (1995)
- K. Li, G. Pang, H.L.W. Chan, C.L. Choy, J.H. Li, *J. Appl. Phys.* **95**, 5691 (2004)
- Y. Zhen, J. Li, *J. Appl. Phys.* **103**, 29 (2008)
- H. Jin, Y. Li, M.S. Song, L. Chen, X.P. Jia, H. An Ma, *Chin. Phys. B* **25**, 534 (2016)
- J. Rödel, K. Webber, R. Dittmer, W. Jo, M. Kimura, D. Damjanovic, *J. Eur. Ceram. Soc.* **35**, 1659 (2015)
- J. Wu, D. Xiao, J. Zhu, *J. Mater. Sci. Mater. Electron.* **26**, 9297 (2015)
- C. Long, T. Li, H. Fan, Y. Wu, L. Zhou, Y. Li, L. Xiao, Y. Li, *J. Alloys Compd.* **658**, 839 (2016)
- J. Xing, Z. Tan, J. Yuan, L. Jiang, Q. Chen, J. Wu, W. Zhang, D. Xiao, J. Zhu, *RSC Adv.* **6**, 57210 (2016)
- D. Xue, J. Gao, Y. Zhou, X. Ding, J. Sun, T. Lookman, X. Ren, *J. Appl. Phys.* **117**, 400 (2015)
- A. Sobhani-Nasab, A. Ziarati, M. Rahimi-Nasrabadi, M. Ganjali, A. Badiei, *Res. Chem. Intermed.* **43**, 6155 (2017)
- M. Rahimi-Nasrabadi, M. Behpour, A. Sobhani-Nasab, S. Hosseinpour-Mashkani, *J. Mater. Sci. Mater. Electron.* **26**, 9776 (2015)
- A. Ziarati, A. Sobhani-Nasab, M. Rahimi-Nasrabadi, M. Ganjali, A. Badiei, *J. Rare Earths* **35**, 374 (2017)
- M. Rahimi-Nasrabadi, M. Behpour, A. Sobhani-Nasab, M. Jeddy, *J. Mater. Sci. Mater. Electron.* **27**, 11691 (2016)
- J. Wang, J.B. Neaton, H. Zheng, V. Nagarajan, S.B. Ogale, B. Liu, D. Viehland, V. Vaithyanathan, D.G. Schlom, U.V. Waghmare, N.A. Spaldin, K.M. Rabe, M. Wuttig, R. Ramesh, *ChemInform* **34**, 1719 (2003)
- W. Eerenstein, F.D. Morrison, J. Dho, M.G. Blamire, J.F. Scott, N.D. Mathur, *Science* **307**, 1203 (2005)
- M. Fiebig, *J. Phys. D* **38**, R123 (2005)
- S. Hunpratub, P. Thongbai, T. Yamwong, R. Yimnirun, S. Maensiri, *Appl. Phys. Lett.* **94**, 062904 (2009)
- I. Sosnowskat, T. Peterlin-Neumaier, E. Steichele, *J. Phys. C* **15**, 4835 (1982)
- R. Palai, R.S. Katiyar, H. Schmid, P. Tissot, S.J. Clark, J. Robertson, S.A.T. Redfern, J.F. Scott, *Phys. Rev. B* **77**, 4110 (2008)
- F.P. Gheorghiu, A. Ianculescu, P. Postolache, N. Lupu, M. Dobromir, D. Luca, L. Mitoseriu, *J. Alloys Compd.* **506**, 862 (2010)
- Z. Yao, C. Xu, H. Liu, H. Hao, M. Cao, Z. Wang, Z. Song, W. Hu, A. Ullah, *J. Mater. Sci. Mater. Electron.* **25**, 4975 (2014)
- R.D. Shannon, *Acta Crystallogr. A* **32**, 751 (1976)
- S. Zhang, Z. Zhang, P. Zheng, M. Zhao, J. Li, C. Wang, *J. Phys. D* **41**, 189801 (2008)
- M.M. Kumar, A. Srinivas, S.V. Suryanarayana, *J. Appl. Phys.* **87**, 855 (2000)
- S.O. Leontsev, R.E. Eitel, *J. Am. Ceram. Soc.* **92**, 2957 (2009)
- M.H. Lee, D.J. Kim, J.S. Park, S.W. Kim, T.K. Song, M.H. Kim, W.J. Kim, D. Do, Il-K. Jeong, *Adv. Mater.* **27**, 6976 (2016)
- Q. Zhou, C. Zhou, H. Yang, C. Yuan, G. Chen, L. Cao, Q. Fan, *J. Mater. Sci. Mater. Electron.* **25**, 196 (2014)
- T. Zhang, Y. Shen, Y. Qiu, Y. Liu, R. Xiong, J. Shi, J. Wei, *ACS Sustain. Chem. Eng.* **5**, 4630 (2017)
- D.-Y. Lu, Y.-Y. Peng, *J. Ceram. Soc. Jpn.* **124**, 455 (2016)